Effective medium theories in electromagnetism for the prediction of water content in cement pastes

Vincent Guihard, Cédric Patapy, Julien Sanahuja, Jean-Paul Balayssac, Frédéric Taillade, Barthélémy Steck

To cite this version:

Vincent Guihard, Cédric Patapy, Julien Sanahuja, Jean-Paul Balayssac, Frédéric Taillade, et al.. Effective medium theories in electromagnetism for the prediction of water content in cement pastes. International Journal of Engineering Science, 2020, 150, pp.103273. ⟨10.1016/j.ijengsci.2020.103273⟩. ⟨hal-02617077⟩

HAL Id: hal-02617077

https://insa-toulouse.hal.science/hal-02617077v1

Submitted on 7 Mar 2022

Version of Record: https://www.sciencedirect.com/science/article/pii/S0020722520300616
Manuscript_42dfbb65f612d8378304a5a932f9022d

Effective medium theories in electromagnetism for the prediction of water content in cement pastes

Vincent Guihard[1,2], Cédric Patapy[2], Julien Sanahuja[3], Jean-Paul Balayssac[2], Frédéric Taillade[1], and Barthélémy Steck[1]

[1] *EDF R&D, PRISME, 6 quai Watier, 78401 Chatou Cedex, France*
[2] *LMDC, Université de Toulouse, INSA, UPS, Génie Civil, 135 Avenue de Rangueil, 31007 Toulouse Cedex 04, France*
[3] *EDF R&D, MMC, Les Renardières, 77818 Moret-sur-Loing Cedex, France*

Corresponding author :
Dr. Vincent Guihard
vincent.guihard@edf.fr
EDF R&D PRISME, 6 quai Watier, 78401 Chatou Cedex, France

Effective medium theories in electromagnetism for the prediction of water content in cement pastes

***[1,2], ***[2], ***[3], ***[2], ***[1], and ***[1]

1 ***

2 ***

3 ***

Abstract

Permittivity is a widespread property used to estimate the water content of heterogeneous materials like concrete. The calibration law employed for the reverse conversion from permittivity to moisture content often relies on time consuming experimental procedures or on empirical equations that do not fit every formulations. To improve the processing of permittivity measurements, we suggest the building of an electromagnetic model of concrete that takes into account the formulation of the material. As a first step, an electromagnetic model for cement pastes is built. This models relies on the knowledge of the formulation and on the use of electromagnetic homogenization schemes. The detailed procedure requires an information about the permittivity of the different phases composing the heterogeneous medium. This paper focuses on the estimation of the dielectric permittivity over the frequency range [200 MHz; 1 GHz] of three of the predominant species present within a cement paste: portlandite, anhydrous cement and C-S-H. This is achieved by synthesising model cementitious binders (C-S-H and portlandite mixtures), by characterizing their macroscopic permittivity with an open-ended coaxial probe and by identifying the intrinsic permittivity of C-S-H and portlandite thanks to a specific homogenization procedure combining effective medium equations. The identified values are eventually used as an entry for homogenization schemes estimating the water content in cement pastes. For a wide range of water content, the simulated and measured real parts of permittivity show a good agreement.

1 Introduction

The delayed mechanical behaviour and the durability properties of concrete depend on its moisture content [1]. The assessment of water content is thus of prime importance for the long term operation of civil engineering structures. While direct measurements are possible, they are destructive by nature, which may not be feasible depending on the targeted structure. Non destructive testing methods are thus of great importance. Due to the relative contrast between liquid, gas and solid properties, permittivity represents an appealing property. It can be acquired, either from embedded sensors (Time Domain Reflectometry [2]) or from the surface using a hand-held probe (capacitive probes [3], coaxial probes [4], Ground Penetrating Radar [5]). A calibration curve is then required to perform the reverse conversion from permittivity to moisture content. Obtaining experimentally such a calibration curve, point per point, requires to successively equilibrate a concrete sample with various relative humidities. At each step, once equilibrium has been reached, permittivity is measured. A large enough sample must be considered, to be representative of concrete, but the larger the sample, the longer the moisture equilibration process. Collecting such an experimental calibration curve can thus be tedious and time consuming, and this process has to be repeated for each different concrete. On the other hand, classical empirical relations (Topp equation [2], Complex Refractive Index Model [6]) tend to lack accuracy as they are not taylored to the specificity of each concrete. Thus, modelling represents an interesting alternative, as it could allow to break down concrete into individual phases whose elementary permittivity is expected to be a unique property from one concrete to another. Macroscopic permittivity of a heterogeneous sample can be approached numerically by averaging the electrical flux through a unit cell defined with periodic boundary conditions [7]. However, in the case of complex multi-scale structures like cementitious materials, time is often a limitation for the use of numerical simulations. Permittivity can then be approached analytically thanks to effective medium theories [8], as developed in this paper. Nevertheless, using effective medium approximations to calculate the macroscopic permittivity of a composite material requires the permittivities and the relative fractions of its components.

In the case of cementitious materials, one major issue for the development of such homogenization model is the lack of information about the permittivity of their components, like the C-S-H gel, portlandite or the anhydrous cement grains. Another issue is the large variety of microstructural models found in the literature [9].

The main anhydrous phase present in cement is $3CaO.SiO_2$ (C_3S). Its crystallographic structure in Portland cement is generally monoclinic due to the presence of impurities in its structure. In the present study, permittivities of Portlandite and anhydrous cement are measured on bulk pellets obtained by compressing commercial powders of the phases. To determine the permittivity of C-S-H, mixes with different C_3S/portlandite ratios were hydrated in order to produce different C-S-H/Portlandite contents. The w/c ratio was optimized to reach a high degree of hydration of C_3S. The different phase contents are evaluated using XRD-Rietveld method with an external standard method. Macroscopic permittivities were measured using an open-ended coaxial probe. The evaluation of porosity by 2-Propanol intrusion porosimetry is necessary for the calculation of the permittivity to take into account the contribution of air/pore solution. The permittivity of each phase is estimated through the use of effective medium theories approaching the relationship between macroscopic permittivity and relative fractions of the components. For C-S-H, a Bruggeman model based homogenization process is used.

Eventually, different ordinary Portland cement pastes were synthesised and characterized. Phases permittivity previously determined are used as inputs in a new homogenization procedure connecting the measured macroscopic permittivity to the amount of water present within the structure.

2 Theory

The relative complex permittivity ϵ_r and the complex electrical conductivity σ (in S/m) are the two main physical parameters used to describe the electromagnetic response of a material. The relative complex permittivity comprises a real part ϵ' characterizing polarization phenomena involved within the medium and an imaginary part ϵ'' characterizing dielectric losses. It can be expressed as $\epsilon = \epsilon' - i\epsilon''$, where $i = \sqrt{-1}$ is the pure imaginary number. The conductivity characterises how weakly that medium opposes the flow of an electric current. Both of those properties come from the definition of the total current density $\mathbf{J_t}$ existing within a medium subject to an applied electrical field $\mathbf{E}$. This current is defined as the sum of a conduction current density $\mathbf{J_c}$ (displacement of free charges) and a displacement current density $\mathbf{J_d}$ (displacement of bound charges). In the case of a harmonic electrical excitation, we have,

$$\mathbf{J_c} = \sigma \mathbf{E} \tag{1}$$

$$\mathbf{J_d} = \frac{\partial \mathbf{D}}{\partial t} = i\omega\epsilon_r\epsilon_0\mathbf{E} \tag{2}$$

where σ is the conductivity, $\mathbf{D}$ is the displacement field, ϵ_0 is the permittivity of free space, $\omega = 2\pi f$ is the angular frequency (in rad.s^{-1}) and t is the time (in s). The total current density can be expressed as,

$$\mathbf{J_t} = \mathbf{J_c} + \mathbf{J_d} = (\sigma + i\omega\epsilon_r\epsilon_0)\mathbf{E} \tag{3}$$

This can be rewritten in order to introduce a global complex permittivity parameter ϵ so that $\mathbf{J_t} = i\omega\epsilon\epsilon_0\mathbf{E}$. Doing so, we have,

$$\epsilon = \epsilon_r - i\frac{\sigma}{\omega\epsilon_0} = \epsilon' - i(\epsilon'' + \frac{\sigma}{\omega\epsilon_0}) \tag{4}$$

As reminded in [10], electrical conductivity σ appears to be the predominant phenomenon at low frequencies. In the case of cementitious materials, the conductivity is strongly dependent on the nature and the amount of ionic species composing the interstitial liquid. Also, at high frequencies, the global complex permittivity appears to be governed by the polarization and dielectric losses phenomena. Every heterogeneity composing the studied composite materials will be characterized in term of its relative complex permittivity, simplified in this paper as "permittivity".

When dealing with heterogeneous media like cementitious materials, the effective permittivity ϵ_{eff} of the medium must be defined. Such macroscopic permittivity results from the contribution of every heterogeneity's permittivity. This property can only be defined in a medium characterized by an overall volume larger than the representative elementary volume (minimum volume for the material to be considered statistically homogeneous).

The effective permittivity of a heterogeneous material is related to the permittivity of its components as well as their relative fraction within the bulk volume. Analytical equations known as effective medium theories [8] have been developed since the past century to approximate the macroscopic permittivity of a composite material from morphological, structural and electromagnetic information about the components. Those models rely on a quasi-static assumption (largest heterogeneity must be small in comparison with the existing electric field's wavelength). Among all models, Bruggeman equation, also known as self-consistent model, symmetrically considers the different phases. Considering a medium made of spheroidal inclusions, the macroscopic permittivity ϵ_{eff} can be derived according to the Bruggeman equation given by,

$$\frac{\frac{1}{3}\sum_{k=1}^{K} f_k(\epsilon_k-\epsilon_{eff}) \sum_{j=x,y,z} \frac{\epsilon_{eff}}{\epsilon_{eff}+N_j(\epsilon_k-\epsilon_{eff})}}{1-\frac{1}{3}\sum_{k=1}^{K} f_k(\epsilon_k-\epsilon_{eff}) \sum_{j=x,y,z} \frac{N_j}{\epsilon_{eff}+N_j(\epsilon_k-\epsilon_{eff})}} = 0 \tag{5}$$

Here, K is the total number of phases and ϵ_k and f_k refer to the permittivity and volumetric fraction of each phase, respectively. Depolarization coefficients N_j enable to take into account the shape of the spheroids in directions (x,y,z). In the case of randomly oriented ones, the aspect ratio a_r is used to estimate the depolarization coefficients. For oblate spheroids ($a_r < 1$), we have,

$$N_x = \frac{a_r}{2}\frac{cos^{-1}(a_r) - a_r\sqrt{1-a_r^2}}{(1-a_r^2)^{3/2}}, \tag{6}$$

With $N_x = N_y$, $N_z = 1 - 2N_x$ and z the axis of revolution. For prolate spheroids ($a_r > 1$), we have,

$$N_x = \frac{a_r}{2}\frac{a_r\sqrt{a_r^2-1} - cosh^{-1}(a_r)}{(a_r^2-1)^{3/2}}, \tag{7}$$

The most common configuration of Bruggeman model relies on a spherical description of the phases' shape ($a_r = 1$ and $N_x = N_y = N_z = 1/3$), giving rise to Eq 8,

$$\sum_{k=1}^{K} f_k \frac{\epsilon_k - \epsilon_{eff}}{\epsilon_k + 2\epsilon_{eff}} = 0 \tag{8}$$

3 Materials and methods

3.1 Measurement of permittivity

Permittivity of materials can be derived from the analysis of transmission and reflection of electromagnetic waves through a sample inserted into a coaxial structure [11] or placed at the end of this structure in the case of reflection only based devices. In this particular case, reflection phenomena are induced by an impedance discontinuity caused by the sample located at the end of a coaxial structure. Open-ended coaxial probes are one of these methods along with many others reviewed in [11] and [12]. They present simple implementation and a broad frequency range driven by the network analyzer used to synthesize the RF signal. The non-destructive and non-invasive characteristics of such tools have enabled investigations of different kinds of media like biological tissues and liquids [13] [14] [12] [15] [16], agricultural products [17] [18], soils [19] [20] [21], and also flat surfaces of solid samples like concrete [22] [23].

In the present study, a probe was designed to investigate the dielectric permittivity of the synthesised samples. It was built by abrading the surface of a N type connector. The built device is characterized by a core radius of 1.2 mm and a metallic shield radius of 4.5 mm. The relatively small radii makes it suitable for the study of tiny samples as well as media characterized by a small representative elementary volume.

The device can be directly connected to a vector network analyser (VNA). The analyser is used to synthesize and deliver the electromagnetic signal, which then propagates within the probe towards the material under test located at its end. The VNA also enables the acquisition of a reflection coefficient associated to the sample and related to its dielectric permittivity thanks to a capacitive model [12]. This model offers immediate permittivity estimation but limit the frequency range investigated [24]. In previous works, modelling of the probe proved its ability to characterize the permittivity of flat media over the frequency range [100 MHz; 1 GHz] [25]. Using such probe and capacitive model also requires a specific calibration procedure detailed in [4].

3.2 Synthesis and characterization of model cementitious binders and cement pastes

3.2.1 CH pellets

Estimating the permittivity of portlandite is achieved by isolating the contribution of portlandite permittivity from the macroscopic permittivity of a mixture made of portlandite and air. These mixtures take the form of small pellets synthesised by conglomerating a pure portlandite powder with a hydraulic press. A total of three solid cylinders with height 5 mm and diameter 20 mm were synthesised. Permittivity measurement of the samples is repeated three times on the surface of each sample with the open-ended coaxial probe. Porosity is then determined to identify the relative fractions of air and portlandite within the samples. For that purpose, cylinders were weighted in air. Then, each sample was dipped into a solution of pure isopropyl alcohol until its mass is stabilized and a complete saturation state is reached. Each sample is then weighted in air and in the isopropyl alcohol solution. Volumetric air fraction ϕ is then calculated from Eq 9 where m_{dry} is the mass of a sample in a dry state, m_{sat} is the mass of a sample saturated with isopropyl alcohol in air and m_{sat}^{iso} is the mass of a sample saturated with isopropyl alcohol in the solution.

$$\phi = \frac{m_{sat} - m_{dry}}{m_{sat} - m_{sat}^{iso}} \tag{9}$$

Averaged porosity obtained is $\phi = 20.2\% \pm 0.5\%$.

3.2.2 Anhydrous Portland cement pellets

A similar procedure is applied to determine the permittivity of an anhydrous Portland cement. A total of three solid cylinders with height 5 mm and diameter 20 mm were synthesised by conglomerating a Portland cement (CEM-I 52.5 N CE CP2 NF). Porosity is determined according to the procedure detailed in Section 3.2.1 ($\phi = 24.3\% \pm$ 0.9%) and macroscopic permittivity is acquired with the open-ended coaxial probe.

3.2.3 C-S-H mixtures

Mixtures of C-S-H and portlandite were synthesised by hydrating a monoclinic phase of a C_3S powder in the presence of portlandite. In order for the resulting material to be reactant-free, water to C_3S mass ratios were optimized (0.42, 0.6 and 0.8). In the following, different mass fractions of reactants are adopted in order to obtain a large variety of products fractions while respecting hydration equation stoichiometry (100 wt% C_3S – 0 wt% CH, 90 wt% C_3S – 10 wt% CH, 80 wt% C_3S – 20 wt% CH).

Experimental protocol consisted in mixing C_3S and portandite powders with pure water and sealing the mixture inside a 20 cL container. Each mixture is synthesised three times to attest the reproducibility of the experiment. Table 1 presents the different mixtures synthesised. Samples are classified according to their water to C_3S mass ratio and according to the fraction of C_3S within the solid reactant volume. Terminology W/C_3S–f_{C_3S} is adopted to characterize each sample. Samples were cured 90 days in sealed containers under saturated conditions. During the curing, the containers were put in a dessicator under nitrogen atmosphere, high relative humidity (>95%) and in the presence of alkali salts to prevent for carbonation.

Porosity of the mixtures was measured thanks a water porosimetry process [26] performed on two out of the three samples for each formulation (except for formulation 06 – 70). As presented in Table 1, porosity is found to be very reproducible. As expected, porosity values increase with the water to C_3S ratio. A relatively small impact of the added CH powder on the measured porosity is observed.

One sample of each formulation was cut in slices of maximum thickness 1 mm. These slices were put in isopropanol during 7 days in order to remove free water and to stop the hydration process. They were then preserved from carbonation and humidity in a partial vacuum using a desiccator. Solid phases were finally manually grinded to a particle size less than $80\mu m$ and analyzed by X-Ray Diffraction (XRD) using a D8 Brucker Diffractometer (Cu radiation; $\lambda K_{\alpha 1,2} = 1.54184$Å) in the Bragg Brentano geometry. XRD data were collected in the range of $2\theta = 5$ř to 70ř, with a 0.0167ř steps. The relative contents of the different solid phases were evaluated by Rietveld refinement (TOPAS software) using an external standard method (rutile) to determine the content of C-S-H (amorphous phase). The CIF files used for the different Rietveld refinement can be found in [27]. Intrinsic density of each element was eventually used to convert weight fractions of the different phases into volumetric fractions. Density of C-S-H was taken equal to 1.96 [28], density of $CaCO_3$ to 2.72, density of CH to 2.24 and density of C_3S to 3.16. Volumetric fractions calculated are also summarized in Table 1. Phases quantification was repeated for 06−70−2 and 06−70−3 samples in order to attest the reproducibility of the synthesis process. All samples tested are composed of C-S-H paste (60 vol% to 71 vol%) and portlandite (23 vol% to 37 vol%). Remaining C_3S does not exceed 1 vol% except for the 042 – 100 mixture (7 vol%). Calcite ($CaCO_3$) does not exceed 2 vol% which proves that carbonation phenomenon was very low.

Information about the morphology of samples' microstructure was obtained thanks to SEM (JEOL 6380 LV) observations in BSE mode of their polished surface. Figure 1 presents a x1000 magnified image of the 06 – 100 mixture.

High density C-S-H blocks (dark grey) are observed spread within a matrix of low density C-S-H (light grey) and surrounding the small amount of remaining anhydrous C_3S (white). During the hydration process of a cement paste, anhydrous cement grains are known to gradually vanish while forming a layer of homogeneous high density C-S-H surrounding them. These layers appear in dark grey in Figure 1. They are characterized by a low capillary porosity and are thus indifferent to drying phenomena below 60°C [29]. In the theoretical case of fully hydrated cement pastes, anhydrous grains would be entirely replaced by the high density C-S-H. In such media, high density C-S-H areas are mixed with portlandite and a low density C-S-H phase composed of C-S-H and high capillary pores containing most of the interstitial liquid (light grey in Figure 1). This distinction between low and high density C-S-H has been used by many authors in the past to describe the microstructure of cement pastes [30] [31]. Following [32] terminology, "*outer*" will now designate low density C-S-H and "*inner*" will designate high density C-S-H.

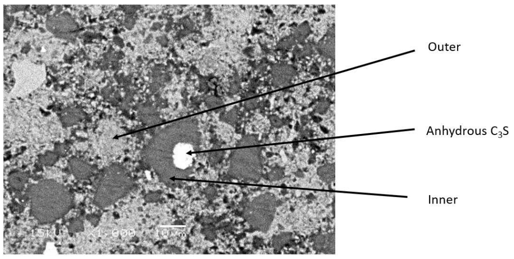

Figure 1: SEM observation of 06-100 sample. Magnification x1000. Backscattered electron mode.

3.2.4 Ordinary Portland cement pastes

Cement pastes were synthesised using the same ordinary Portland cement (OPC) as presented in Section 3.2.2 (CEM-I 52.5 N CE CP2 NF). The samples take the form of cubes with length equal to 8 cm. Different volumes of water were added to the mixtures in order to get a wide enough porosity spectrum and evaluate the previously derived results on different formulations. The water to cement mass ratios are chosen equal to 0.28, 0.34 and 0.40. Three samples were synthesized for each formulation, leading to a total of nine samples. A 28 days curing period in a water saturated environment is applied to all samples. One out of the three samples for each formulation is subjected to porosity measurement following the procedure described in [26]. Quantitative XRD is also performed on each sample in order to determine the volumetric fraction of the solid phases. Porosity results are presented in Table 2. Volumetric fractions of the solid phases are presented in Table 3. It can be noticed that as the water to cement mass ratio decreases, the volumetric fraction of anhydrous cement increases. Also, whatever the formulation, C-S-H appears to be the main specie present within the samples. Calcite was also observed on a minor fraction.

A total of three permittivity measurements are repeated on three out the six faces of each cube for reproducibility evaluation at different degrees of saturation. Starting from a completely saturated state, every sample is dried in an oven at 60°C while monitoring the mass decrease. From the knowledge of the sample's porosity, the mass decrease is associated to a decrease in the degree of saturation of the material. Each time a sample loses 10% of degree of saturation, it is removed from the oven, its faces are covered with an adhesive aluminium foil and the sample is put back in the oven for an amount of time corresponding to the time needed to reach the targeted saturation degree. This process should ensure a uniform local saturation degree and thus a homogeneous permittivity within the sample. After cooling, the aluminium foil is removed and the open-ended coaxial probe is once again used to measure the permittivity of the sample. Such drying and permittivity measurement procedure is repeated until samples' mass is stabilized for that specific temperature (approximately one month). Doing so, the complex permittivity spectra of the ordinary Portland cement pastes are acquired for different degrees of saturation. Those spectra are to be compared with the modelled permittivity of the cement pastes.

3.3 Morphological modelling and estimation of the effective permittivity

3.3.1 CH and anhydrous Portland cement pellets

In the case of a two phase medium like the CH pellets (portlandite and air) or the anhydrous Portland cement pellets (cement and air), the material can be modelled as randomly oriented spheroidal inclusions of solid and air. The Figure 2 illustrates the special case of spherical inclusions of air and portlandite. This geometry is firstly adopted to identify the effective permittivity of the synthesized pellets. The assessment of the macroscopic permittivity of CH pellets ϵ_{eff} through open-ended coaxial probe measurement will enable to identify the permittivity of portlandite ϵ_{CH} (the solid part of the composite medium). An identical model can be used to identify the permittivity of anhydrous cement from the built pellets presented in Section 3.2.2.

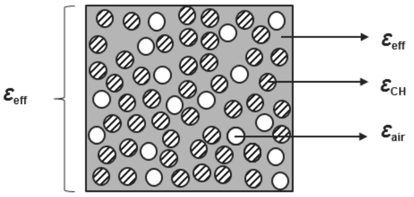

Figure 2: Geometry adopted to estimate the effective permittivity of portlandite according to the Bruggeman model.

3.3.2 C-S-H mixtures

Modelling the effective permittivity of C-S-H based mixtures with effective medium theories is more challenging than for portlandite pellets. The complex composition and morphology of the synthesised materials observed in Figure 1 limits the use of a single Bruggeman model. SEM observation is here used to model the effective permittivity of the C-S-H based mixtures, combined with the assumption that C_3S was fully reacted and that calcite was non-existent. This is justified by the very low volumetric fraction determined in section 3.2.3. Following such hypothesis, volumetric fractions of portlandite and C-S-H can

Table 1: Summary of all samples synthesised according to their formulation.

Sample	W/C_3S	C_3S (wt%)	CH (wt%)	Porosity (%)	CH (vol%)	$CaCO_3$ (vol%)	C-S-H (vol%)	C_3S (vol%)
08-100-1	0.8	100	0	48.9	-	-	-	-
08-100-2	0.8	100	0	48.4	-	-	-	-
08-100-3	0.8	100	0	-	28	0	71	1
08-90-1	0.8	90	10	47.6	-	-	-	-
08-90-2	0.8	90	10	47.8	-	-	-	-
08-90-3	0.8	90	10	-	34	2	64	1
08-80-1	0.8	80	20	46.3	-	-	-	-
08-80-2	0.8	80	20	45.9	-	-	-	-
08-80-3	0.8	80	20	-	37	2	60	0
06-90-1	0.6	90	10	38.4	-	-	-	-
06-90-2	0.6	90	10	38.4	-	-	-	-
06-90-3	0.6	90	10	-	32	1	65	1
06-70-1	0.6	70	30	39.0	-	-	-	-
06-70-2	0.6	70	30	-	36	2	60	1
06-70-3	0.6	70	30	-	36	2	60	1
042-100-1	0.42	100	0	28.9	-	-	-	-
042-100-2	0.42	100	0	28.9	-	-	-	-
042-100-3	0.42	100	0	-	23	0	70	7

Table 2: Summary of all OPC samples synthesised according to their formulation and their measured porosity.

Sample	W/C	Porosity (%)
028-1	0.28	26.7
028-2	0.28	26.5
034-1	0.34	31.7
034-2	0.34	31.8
040-1	0.40	35.9
040-2	0.40	36.0

Table 3: Summary of the phases in OPC samples and their volumetric fraction determined through quantitative XRD.

Species	Density	$028-1$	$034-1$	$040-1$
C_3S	3.17	4%	4%	3%
C_2S	3.33	5%	4%	4%
C_3A	3.02	0%	0%	0%
C_4AF	3.71	2%	2%	1%
$Ca(OH)_2$	2.25	13%	13%	13%
Ettringite	1.78	6%	6%	6%
Monosulfo-aluminate	1.99	1%	1%	1%
Gypsum	2.31	1%	1%	1%
Quartz	2.64	1%	1%	1%
Calcite	2.72	3%	3%	3%
Hemicarbo-aluminate	1.99	1%	1%	1%
C-S-H	1.96	64%	65%	66%

Table 4: Simplified relative fractions of C-S-H and CH within the solid part of the synthesised mixtures.

Sample	CH (vol%)	C-S-H (vol%)
08-100	28	72
08-90	34	66
08-80	38	62
06-90	33	67
06-70	43	57
042-100	25	75

be extrapolated to the whole solid volume of each mixture, leading to the relative fractions presented in Table 4. Even though C-S-H paste is porous and contains water, its permittivity will be assumed real and constant over the specific frequency range studied. This assumption comes from the fact that water molecules in C-S-H pores are chemically linked to C-S-H sheets, giving them a permittivity close to a solid's one [33], with limited impact of the ionic species on the permittivity dispersion. Despite an overall knowledge of the mixtures' morphology, different geometries can be adopted to model their effective permittivity with homogenization schemes. In this paper, the suggested geometry relies on the following assumptions:

- The C-S-H gel, whether it is located within the *inner* or the *outer* part of the microstructure, is considered as a homogeneous phase of the medium, with a constant permittivity whatever the mixture's formulation.
- *Inner* phase capillary porosity is assumed to be null. In this way, *inner* phase is assumed to be exclusively made of C-S-H.
- All capillary pores are located within the *outer* phase of the microstructure. This phase is composed of C-S-H paste and capillary pores.
- When the hydration is complete, the volume occupied by the *inner* phase is equal to the initial volume of anhydrous reactant, before hydration.

The homogenization process adopted in this paper consists in a successive application of two effective medium approximations. First, permittivity of the *outer* phase is obtained by mixing the permittivity of spherical inclusions of C-S-H and pores thanks to the Bruggeman equation. The resulting permittivity is then mixed with the permittivity of C-S-H, modelling the *inner* phase, and with the permittivity of CH in order to estimate the macroscopic permittivity of the mixture. In the present study, permittivity measurement were realized on saturated samples. Pores can thus be assimilated as an interstitial solution phase. The suggested process is illustrated in Figure 3. Using such geometry implies that the relative fraction of C-S-H paste included within the *inner* and the *outer* part is known. This information comes from the assumption that hydration is complete and that the volume occupied by the *inner* phase is equal to the initial volume of anhydrous reactant, before hydration. Following the procedure developped by Sanahuja et al. [34], Powers model [35], presented in Eq 10, can be employed to estimate the fraction of anhydrous cement f_a in a cement paste, as a function of the ongoing hydration process. The degree of hydration is denoted α and W/C is the water to cement mass ratio. Using such parameters, we get,

$$f_a = \frac{0.32(1-\alpha)}{W/C + 0.32} \tag{10}$$

We now assume that the created volume of the *inner* phase after complete hydration is equal to the anhydrous phase fraction when $\alpha = 0$, leading to,

$$f_{inner} = \frac{0.32}{W/C + 0.32} \tag{11}$$

The fraction of *outer* within the overall volume is then given by $f_{outer} = 1 - f_{CH} - f_{inner}$, where f_{CH} is the fraction of portlandite determined by quantitative XRD. Summary of the fraction of each phase is presented for the two successive homogenization steps in Table 5 and Table 6. Those values are to be combined with the measured effective permittivity through the successive Bruggeman models, enabling the identification of the C-S-H paste permittivity.

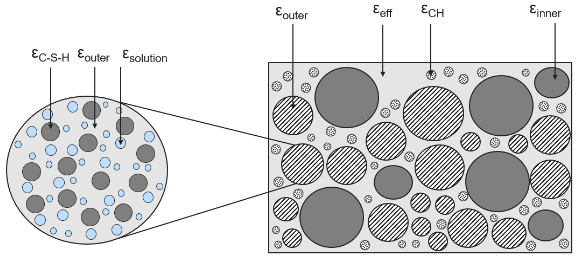

Figure 3: Adopted geometry used to model the morphology of the synthesised C-S-H based mixtures.

Table 5: Parameters required for the calculation of the *outer* permittivity ϵ_{outer} (First homogenization step).

Outer		
Phase	C-S-H	Solution
Fraction	$1 - \phi/f_{outer}$	ϕ/f_{outer}
Permittivity	ϵ_{CSH}	$\epsilon_{solution}$
Aspect ratio a_r	1	1

Table 6: Parameters required for the calculation of the effective permittivity of the mixture ϵ_{eff} (Second homogenization step).

Inner, portlandite and outer			
Phase	Inner	CH	Outer
Fraction	f_{inner}	f_{CH}	f_{outer}
Permittivity	ϵ_{CSH}	ϵ_{CH}	ϵ_{outer}
Aspect ratio a_r	1	1	1

In the detailed homogenization process, electromagnetic properties of the interstitial solution ϵ_{sol} are still to be investigated in order to identify the permittivity of C-S-H paste. In this present study, a Debye equation [36] is used to model its dielectric dispersion. This model is classically used to describe the evolution of conductive water permittivity below 100 GHz. It is defined as,

$$\epsilon_r = \epsilon_\infty + \frac{\epsilon_{stat} - \epsilon_\infty}{1 + i\omega\tau} + \frac{\sigma}{i\omega\epsilon_0} \tag{12}$$

where ϵ_{stat} and ϵ_∞ are the limit of permittivity at low and high frequencies, respectively equal to 80 and 3.13. τ is the relaxation time of pure water ($\tau = 10^{-11}$ s), σ the DC ionic conductivity and ϵ_0 the permittivity of free space. Real and imaginary part of the permittivity of capillary water are known to be a function of the ionic concentration. This is true for dilute solutions, with a real part ranging from 60 to 80 [37]. DC conductivity of the synthesised samples was not investigated in the present study and will be optimized.

3.3.3 Ordinary Portland cement pastes

The permittivity model of the C-S-H mixtures can now be extended to the case of ordinary Portland cement pastes through minor modifications. Concerning all cement pastes, XRD quantification presented in Section 3.2.4 indicates that, contrarily to C-S-H mixtures, the remaining anhydrous components (C_3S, C_2S, C_3A, C_4AF and gypsum) can no longer be assumed non-existent. Minor components like ettringite, monosulfoaluminate, hemicarboaluminate, calcite and quartz will be neglected, assuming that their permittivity has a non critical influence on the macroscopic sample's permittivity. Their fraction is around 10% of the total volume, whatever the formulation. Volumetric fraction of C-S-H, portlandite and anhydrous components are extrapolated to the entire volume, as if they were the only components, leading to the simplified summary of the species presented in Table 7. Another difference with the model built for C-S-H mixtures is the introduction of the unsaturated state of the samples. As the degree of saturation of the OPC cement decreases during the drying process, interstitial water is gradually replaced by air. The suggested geometry adopted to model OPC permittivity then consist in three different homogenization steps described below and illustrated in Figure 4.

Table 7: Simplified summary of the species composing the cement pastes.

Phase	$W/C0.28$	$W/C0.34$	$W/C0.4$
Anhydrous	13%	12%	11%
$Ca(OH)_2$	15%	15%	16%
C-S-H	72%	73%	73%

- Outer phase permittivity is calculated using a Bruggeman model with spherical inclusions of C-S-H and spherical inclusions of pore (either air or water depending on the degree of saturation).
- Inner phase permittivity is calculated using a Bruggeman model with spherical inclusions of C-S-H and spherical inclusions of anhydrous cement.
- The effective permittivity of the material is calculated using a Bruggeman model with spherical inclusions of portlandite, inner and outer phases.

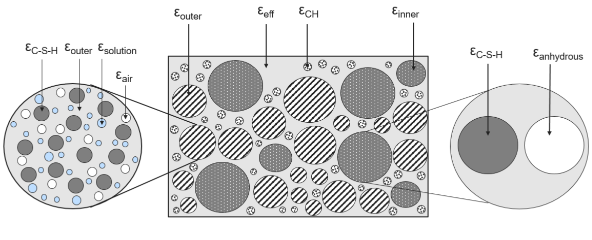

Figure 4: Adopted geometry used to model the morphology of the synthesised cement pastes.

An information about phases repartition whithin the inner and outer phases is then required to evaluate the effective permittivity. Since the remaining fraction of anhydrous cement is not equal to zero, Powers model is no longer used alone to estimate the distribution of C-S-H between the inner and outer phases. According to Tennis and Jennings [30], C-S-H distribution can be expressed as a function of the degree of hydration α and the water to cement mass ratio W/C. γ is defined as the inner phase mass ratio in a cement paste (Eq 13).

$$\gamma = 3.017\alpha W/C - 1.347\alpha + 0.538 \tag{13}$$

Powers model (10) is then used to estimate the degree of hydration α from the remaining anhydrous fraction (estimated through quantitative XRD). Eventually, the C-S-H paste located within the inner and outer phases being of the same density [34], mass fractions can be directly expressed in terms of volumetric fractions. Volumetric fraction of the C-S-H paste within the outer phase f^o_{CSH} can thus be expressed as the function of the volumetric fraction of C-S-H in the samples f^{tot}_{CSH} and according to Eq 14,

$$f^o_{CSH} = \gamma f^{tot}_{CSH} \tag{14}$$

Volumetric fraction of the C-S-H paste within the inner phase f^i_{CSH} is then expressed as the difference between the volumetric fraction of C-S-H paste within the sample and the volumetric fraction of the C-S-H phase within the outer phase. Eventually, all phases distribution according to the built model are summarized in Table 8 according to the degree of saturation S, the total porosity ϕ, the volumetric fraction of the C-S-H paste within the outer phase f^o_{CSH}, the volumetric fraction of the C-S-H within the inner phase f^i_{CSH}, the volumetric fraction of the remaining anhydrous cement f_a and the volumetric fraction of portlandite in the sample f_{CH}.

Table 8: Phases distribution according to the built homogenization model of the ordinary Portland cement pastes.

Step	outer C-S-H and pores			inner C-S-H and anhydrous cement		CH
Phase	outer C-S-H	Water	Air	Anhydrous	inner C-S-H	CH
Fraction	$\frac{f^o_{CSH}}{f^o_{CSH}+\phi}$	$\frac{S\phi}{f^o_{CSH}+\phi}$	$\frac{(1-S)\phi}{f^o_{CSH}+\phi}$	$\frac{f_a}{f_a+f^i_{CSH}}$	$\frac{f^i_{CSH}}{f_a+f^i_{CSH}}$	f_{CH}

4 Results and discussion

4.1 Measurement of the permittivity of the mixtures

The permittivity spectrum of the CH pellets was acquired over the frequency range [10 MHz; 1 GHz] with the coaxial probe, as presented in Figure 5. A slight deviation is observed for frequencies below 100 MHz. Both real and imaginary parts of the permittivity spectrum remains constant for frequencies ranging between 100 MHz and 1 GHz. In the following, imaginary part of the permittivity is assumed to be null and the real part constant and equal to 5.6 ± 0.2 (mean value over [100 MHz; 1 GHz]).

The permittivity spectrum acquired on the anhydrous Portland cement pellets was acquired over the frequency range [10 MHz; 1 GHz] with the coaxial probe, as presented in Figure 6. Both real and imaginary parts of the permittivity spectrum remains constant over the whole frequency range. In the following, imaginary part of the permittivity is assumed to be null and the real part constant and equal to 6.3 ± 0.2 (mean value over [100 MHz; 1 GHz]).

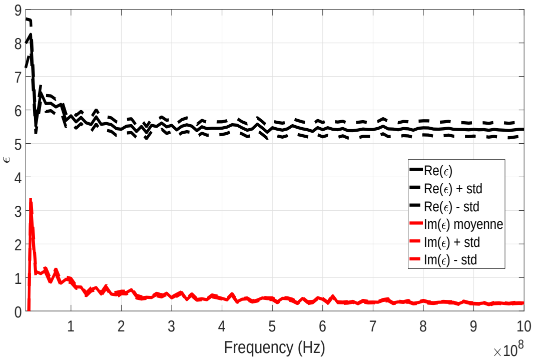

Figure 5: Real and imaginary part of permittivity of the CH pellets. Standard deviation is calculated from reproducibility measurements performed on the samples.

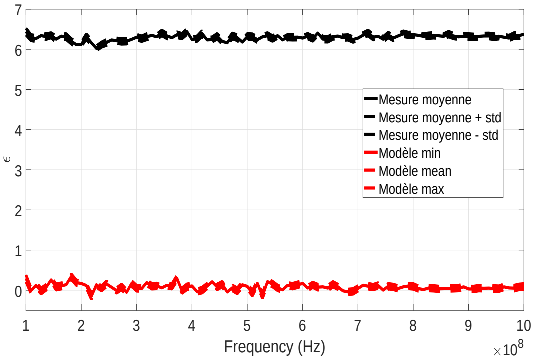

Figure 6: Real and imaginary part of permittivity of the anhydrous Portland cement pellets. Standard deviation is calculated from reproducibility measurements performed on the samples.

About the saturated C-S-H mixtures, their permittivity is acquired within the range [10 MHz; 1 GHz] at two different positions. Figure 7 and 8 present the mean value of the real and imaginary parts for three different formulations characterized by different water to C_3S ratios. A strong frequency dependency is observed on both the real and imaginary parts. This effect is caused by the high amount of conductive interstitial solution present within the pore structure of the saturated samples. Therefore, dielectric properties cannot be averaged and the permittivity should be treated in its complex form in order to identify the permittivity of C-S-H. Also, it can be noticed that the higher the porosity, the higher the real part of permittivity. This is consistent with the fact that samples are saturated and that from all components of the mixtures, capillary water is characterized by the highest permittivity over this frequency range.

Permittivity measurements performed on the cement pastes reveal a strong dependency in the water content, as illustrated in Figure 9 and 10. Both real and imaginary parts systematically increase with the degree of saturation. This is consistent with the permittivity of water being the highest compared to the other phases encountered within the material. A frequency dependence is also

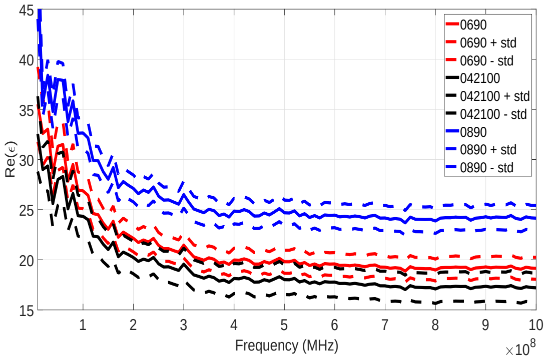

Figure 7: Real part of permittivity of the C-S-H based samples.

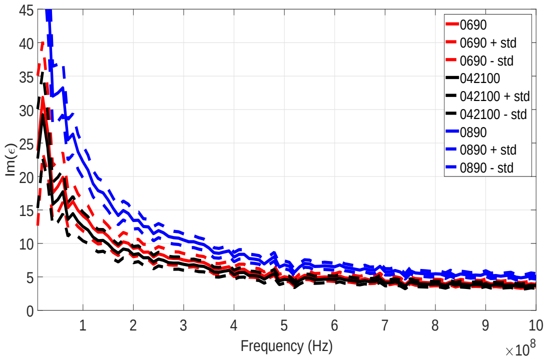

Figure 8: Imaginary part of permittivity of the C-S-H based samples.

observed on both real and imaginary parts of the permittivity, especially at low frequencies and for high water contents.

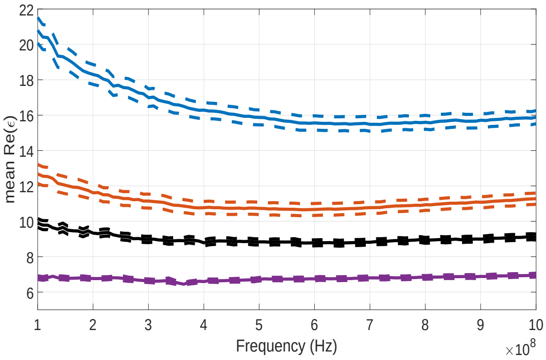

Figure 9: Averaged real part of permittivity of the cement pastes with water to cement ratio 0.28 at different saturation degrees: 100% (blue), 78% (red), 58% (black) and 19% (purple). The dashed lines represents the mean values plus or minus the standard deviation.

4.2 Identification of the permittivity of CH and ordinary Portland cement

Portlandite pellets are made of air and solid portlandite. Permittivity of air is equal to 1 and the macroscopic permittivity as well as the volumetric fraction of the components have been experimentally derived in section 4.1 and 3.2.1. They are equal to 5.6 ± 0.2 and 20.2% ± 0.5%, respectively. As presented in section 3.3.1, a Bruggeman model can be used to calculate the permittivity of portlandite. Eq 5 was solved for a total 10000 values of sample porosity and macroscopic permittivity, normally distributed around their mean value and assumed uncorrelated, following a Monte-Carlo procedure. Deduced portlandite permittivity is found to follow a Gaussian distribution. Finally a value of $\epsilon_{CH} = 7.4 \pm 0.3$ is obtained. Effect of the shape of both portlandite and air phases through the Bruggeman model was tested. Aspect ratio of the inclusions was changed from 1 to 0.1 and 10. Impact on the calculated portlandite permittivity is found to be negligible.

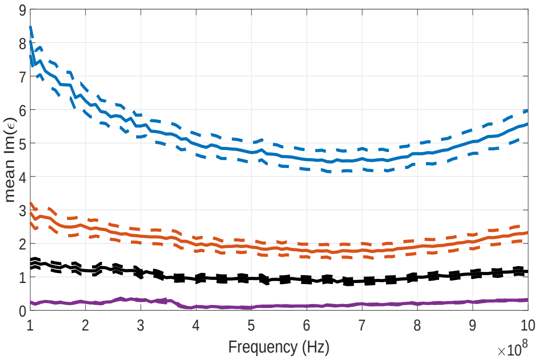

Figure 10: Averaged imaginary part of permittivity of the cement pastes with water to cement ratio 0.28 at different saturation degrees: 100% (blue), 78% (red), 58% (black) and 19% (purple). The dashed lines represents the mean values plus or minus the standard deviation.

A similar experiment is performed with cement pellets data. An approximation of Portland cement grains permittivity is obtained. We have $\epsilon_{anhydrous} = 9.1 \pm 0.3$. Similarly to portlandite, no effect of the particles aspect ratio was observed.

4.3 Identification of the permittivity of C-S-H

The homogenization procedure presented in section 3.3.2 simulates the effective permittivity of the synthesised samples for a given set of known and unknown parameters. The permittivity of C-S-H as well as the DC conductivity of interstitial water remains unknown. Their values are optimized in order for the effective permittivity to match the measured one. To do so, an optimization algorithm based on the least squares method was implemented. The values of C-S-H permittivity and interstitial solution conductivity minimizing the deviation between the measured effective permittivities and the simulated ones over the frequency range [10 MHz; 1 GHz] are searched. According to the assumption that the permittivity of C-S-H is the same whatever the mixture's formulation, the optimization combines every sample at the same time. However, DC conductivity of the water varies from one sample to another. Lower and upper bounds for the C-S-H permittivity are set to $\epsilon_{CSH}^{min} = 2$ and $\epsilon_{CSH}^{max} = 20$, even though no change was observed for a larger range. Similarly, lower and upper bounds for the solution conductivities are set to $\sigma_{solution}^{min} = 0.2$ S/m and $\sigma_{solution}^{max} = 5$ S/m.

Optimization was performed on three different samples' formulations simultaneously ($042-100$, $06-90$ and $08-90$), requiring a reasonable computation time (less than 15 min on a standard laptop) and covering a large scope of water to C_3S mass ratio. Figure 11, 12 and 13 present, for each formulation, the optimized effective permittivity, compared with measurement. The optimized set of permittivity and conductivity values used are $\epsilon_{CSH}=4.81$, $\sigma_{042100}=1.18$ S/m, $\sigma_{0690}=0.69$ S/m and $\sigma_{0890}=0.60$ S/m.

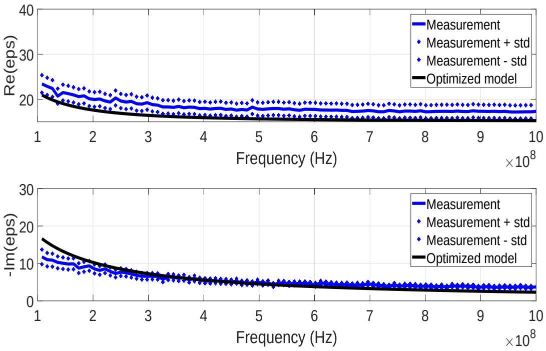

Figure 11: Measured permittivity of $042-100$ sample over the range [10 MHz; 1 GHz] and comparison with optimized effective permittivity ($\epsilon_{CSH}=4.8$ and $\sigma_{042100}=1.18$ S/m). Mean squared error between the real part simulated and measured is 11.0%.

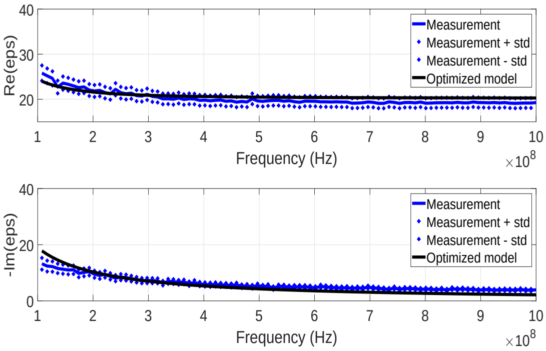

Figure 12: Measured permittivity of $06-90$ sample over the range [10 MHz; 1 GHz] and comparison with optimized effective permittivity ($\epsilon_{CSH}=4.8$ and $\sigma_{0690}=0.69$ S/m). Mean squared error between the real part simulated and measured is 6.0%.

So far, a spherical description of water and air inclusions morphology was adopted within the homogenization scheme. Aspect ratio of those phases was changed from 1 to 0.1, 0.01, 10 and 100. Impact on the mean squared error between the simulations and measurements is found to be negligible.

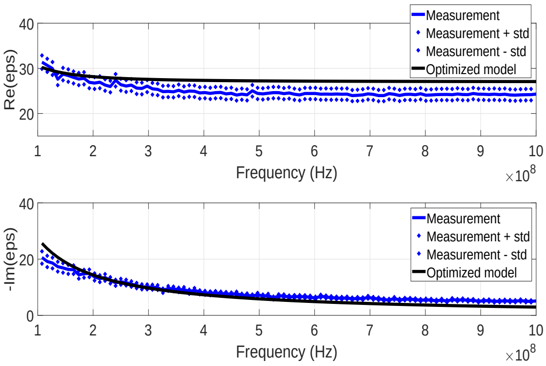

Figure 13: Measured permittivity of $08-90$ sample over the range [10 MHz; 1 GHz] and comparison with optimized effective permittivity ($\epsilon_{CSH}=4.8$ and $\sigma_{0890}=0.60$ S/m). Mean squared error between the real part simulated and measured is 11.1%.

It can also be noticed that the optimized solutions conductivity decreases as the water to C_3S mass ratio increases. Higher ratios leading to higher porosity values, it can be suggested that ionic species present within the pore volume are more diluted in high porosity samples. Consequences would be a decrease in the DC conductivity of the interstitial water.

4.4 Discussion: an application to OPC systems

4.4.1 Effect of the frequency on the calculated effective permittivity

The estimated permittivity of the main components of ordinary Portland cement pastes are summarized in Table 9. Those values are used as inputs in the homogenization procedure detailed in Section 3.3.3, with volumetric fraction of the different phases estimated through quantitative XRD in Section 3.2.4. The effective permittivity calculation is repeated for 100 different frequencies ranging from 100 MHz to 1 GHz and for several degrees of saturation ranging from a completely dry state ($S=0$) to a completely saturated state ($S=1$). This whole process is repeated for each of the three paste formulations ($W/C=0.28$, $W/C=0.34$ and $W/C=0.40$). In a first time, water DC conductivity used in the Debye model is arbitrary chosen equal to 1.0 S/m. The simulated real and imaginary parts of permittivity are presented in

Table 9: Summary of the estimated permittivities of the main components of the ordinary Portland cement pastes.

Phase	Permittivity
C-S-H	4.8
Water	Debye
Air	1
Anhydrous cement	9.0 ± 0.3
Portlandite	7.4 ± 0.3

Figure 14 and 15 for the $W/C = 0.34$ formulation and for four different degrees of saturations. It can be noticed that as the degree of saturation increases, both the real and imaginary parts of permittivity increases. A strong frequency dependence is observed on the imaginary part. This deviation increases with the degree of saturation. A non-negligible deviation of the real part of permittivity is also observed for highly saturated samples and for frequencies below 400 MHz.

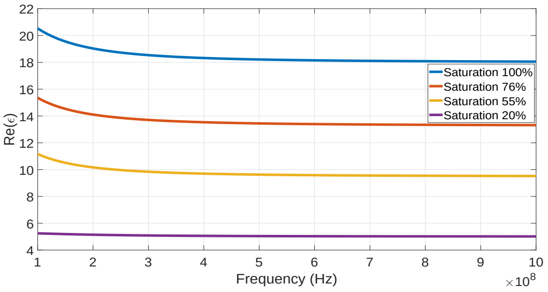

Figure 14: Simulated real part of permittivity of the $W/C = 0.34$ cement paste at different degrees of saturation : 100% (blue), 76% (orange), 55% (yellow), 20% (purple).

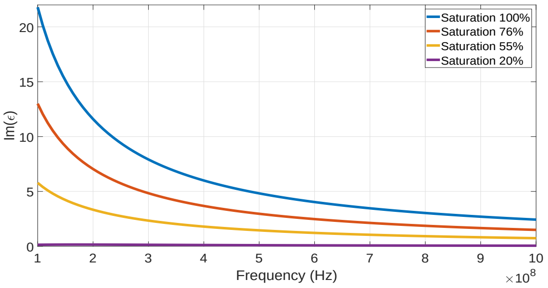

Figure 15: Simulated imaginary part of permittivity of the $W/C = 0.34$ cement paste at different degrees of saturation : 100% (blue), 76% (orange), 55% (yellow), 20% (purple).

4.4.2 Effect of the water DC conductivity on the calculated effective permittivity

The effect of water DC conductivity on the effective permittivity was studied. The arbitrary value of 1.0 S/m was successively changed to 2.0 S/m and 3.0 S/m. A strong effect is observed on both the real and the imaginary parts of the calculated permittivity, as illustrated in Figures 16 and 17. Low frequency imaginary part of permittivity strongly increases as the DC conductivity of water increases. Low frequency real part of permittivity also increases with the DC conductivity. However, for sufficiently high frequencies, this effect vanishes and the real part of permittivity tends toward a constant value. Because of the lack of information about the DC conductivity of the synthesized samples, this property is chosen equal to 1.0 S/m for every simulation. In the following, due to this lack of information, the study will focus on the real part of permittivity. In this way, its mean value over a specific frequency range can be compared with measurement from different devices (GPR, TDR).

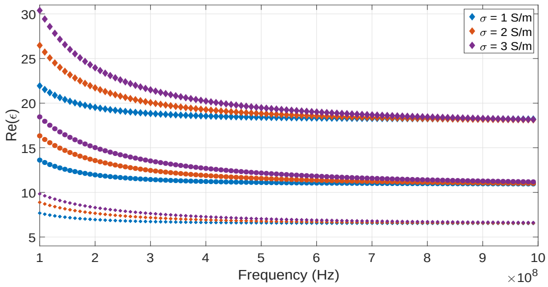

Figure 16: Simulated real part of permittivity of the $W/C = 0.34$ cement paste for three DC conductivity of water values and for three different degrees of saturations : 100% (diamond), 76% (dot), 20% (cross).

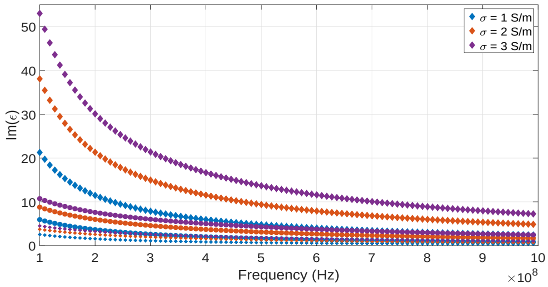

Figure 17: Simulated imaginary part of permittivity of the $W/C = 0.34$ cement paste for three DC conductivity of water values and for three different degrees of saturations : 100% (diamond), 76% (dot), 20% (cross)..

4.4.3 Effect of the aspect ratio of pore inclusions on the calculated effective permittivity

The shape of water and air inclusions is now changed from spheres to spheroids with different aspect ratios ranging from 0.001 to 1000. Averaged value of the real part of permittivity over the frequency range [400 MHz; 800 MHz] is presented as a function of the degree of saturation in Figure 18 for different pores inclusions aspect ratios for the case of the $W/C = 0.34$ formulation. When pores are described as oblate spheroids or discs ($a_r < 1$), the permittivity slope is stronger for higher degrees of saturation. This is not the case when pores are described as prolate spheroids or needles ($a_r > 1$). In that particular case, the slope of the curve tends to be constant as the aspect ratio increases. It can then be suggested that prolate spheroids, characterized by a smaller specific surface will minimize the interaction between pore inclusions. On the other hand, oblate spheroids, characterized by a larger specific surface, will maximize their intersection and therefore their interaction. As it was already the case in Section 4.3 for C-S-H based mixtures, no effect of pores inclusions shape on the calculated permittivity is observed in saturated conditions ($S = 1$). In a percolated system such as a cementitious material, porosity interconnection is maximal. Therefore, a disc-like description of inclusions ($a_r < 1$) is adapted to model both air and water filled pores.

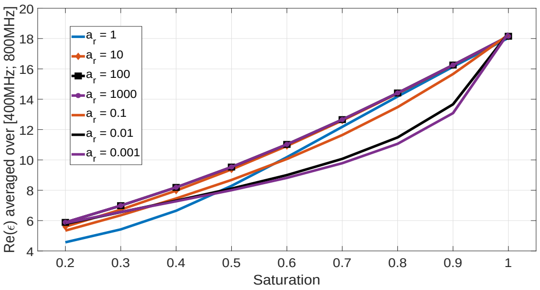

Figure 18: Real part of permittivity averaged over [400 MHz; 800 MHz], for the case of a $W/C = 0.34$ formulation and for different aspect ratio a_r of the pore inclusions.

4.4.4 Comparison with experimental results

The permittivity model developed for cement pastes was solved 1000 times following a Monte-Carlo procedure with the permittivity of the components and the porosity of the samples normally distributed around their mean value. The aspect ratio of pore inclusions is chosen equal to 0.001 and the DC conductivity of water is taken equal to 1.0 S/m. The calculated effective permittivity is found to follow a Gaussian distribution. The good agreement between simulated and measured real parts of permittivity is illustrated in Figure 19 for the $W/C = 0.34$ formulation. Also, averaged values over the frequency range [400 MHz; 800 MHz] are compared with the experimental ones in Figure 20, 21 and 22 for every formulation (0.28, 0.34 and 0.40, respectively). The good agreement between simulations and measurements validates the developed model for cement pastes. In addition, those figures present a comparison between the experimental data and basic three phase Bruggeman and Maxwell-Garnett models (solid, air and water). For those models, nor the frequency dependence of the water permittivity nor the multi-scale morphology of the medium was taken into account in the homogenization procedure. Volumetric fractions and permittivities of the three phases are presented in Table 10 as a function of the material's porosity ϕ and degree of saturation S. Permittivity of the solid phase is chosen to minimize the deviation between simulation and measurements. For the three phase Maxwell-Garnett simulation, the solid phase is the host medium. Compared to these two models, the effective permittivity of the cement pastes estimated with the new model is more consistent with experimental results. From the knowledge of a cement paste formulation and thanks to the measurement of its dielectric permittivity, the new model developed can be used to estimate its water saturation degree.

Table 10: Permittivity and volumetric fractions of the phases used in the three-phase Bruggeman and Maxwell-Garnett models.

Phase	Solid	Liquid	Air
Permittivity	8	80	1
Volumetric fraction	$1 - \phi$	ϕS	$\phi(1 - S)$

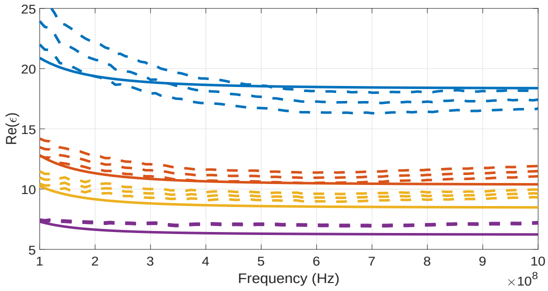

Figure 19: Real part of permittivity measured and simulated for the $W/C = 0.34$ formulation. Results are presented for different degrees of saturation: 100% (blue), 76% (orange), 55% (yellow), 20% (purple).

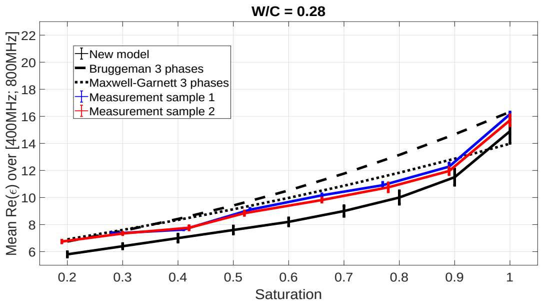

Figure 20: Averaged value over [400 MHz; 800 MHz] of the real part of permittivity measured and simulated for the $W/C = 0.28$ formulation. Comparison with a three-phase Bruggeman and Maxwell-Garnett models.

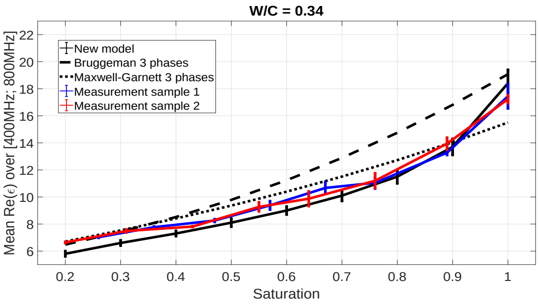

Figure 21: Averaged value over [400 MHz; 800 MHz] of the real part of permittivity measured and simulated for the $W/C = 0.34$ formulation. Comparison with a three-phase Bruggeman and Maxwell-Garnett models.

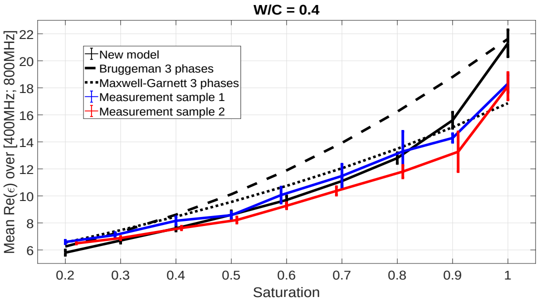

Figure 22: Averaged value over [400 MHz; 800 MHz] of the real part of permittivity measured and simulated for the $W/C = 0.40$ formulation. Comparison with a three-phase Bruggeman and Maxwell-Garnett models.

5 Conclusion

The study presents an electromagnetic model for cement pastes. The procedure employed to build the model relies on the estimation of the dielectric permittivity of portlandite, C-S-H gel and anhydrous cement as parameters for the estimation of water content in cement pastes. The developed procedure comprises the synthesis of samples with elementary composition, their electromagnetic characterization with an open-ended coaxial probe and the use of effective medium theories. A Bruggeman equation is used to identify the permittivity of portlandite from the measurement of the macroscopic permittivity of mixtures made of portlandite and air. Estimated permittivity is $\epsilon_{CH} = 7.4 \pm 0.3$. The same procedure is applied to determine the permittivity of ordinary Portland cement grains. Estimated permittivity is $\epsilon_{anhydrous} = 9.0 \pm 0.3$. Mixtures of C-S-H, portlandite and interstitial water were synthesised by hydrating a mono-clinical phase of a C_3S powder in the presence of portlandite. A specific combination of two Bruggeman equations enabled to optimize the permittivity of C-S-H paste from a measurement of the macroscopic permittivity of the synthesised samples. The resulting value is $\epsilon_{CSH} = 8.0$. Eventually, simulated permittivity of OPC pastes with a specific multi-scale combination of three Bruggeman equations enabled to connect the amount of water within the pore medium and the macroscopic permittivity of the synthesised samples. The designed model presents a better agreement with experimental data than a simple three phases Bruggeman or Maxwell-Garnett model with air, solid and water inclusions. In the future, the model developed for cement pastes will be extended to the case of mortar and concrete by adding a last homogenization step in order to take into account the aggregates in the material's formulation.

References

[1] Z. Zhang, M. Thiery, and V. Baroghel-Bouny. Investigation of moisture transport properties of cementitious materials. *Cement and Concrete Research*, 89, 11 2016. 1

[2] G.C. Topp and J.L. Davis. Time-domain reflectometry (tdr) and its application to irrigation scheduling. *Advances in Irrigation*, 3:107–127, 12 1985. 1

[3] G. Villain, A. Ihamouten, and X. Dérobert. Determination of concrete water content by coupling electromagnetic methods: Coaxial/cylindrical transition line with capacitive probes. *NDT & E International*, 88, 02 2017. 1

[4] V. Guihard, F. Taillade, J.P. Balayssac, B. Steck, and J. Sanahuja. Modelling the behaviour of an open-ended coaxial probe to assess the permittivity of heterogeneous dielectrics solids. *Progress In Electromagnetics Research Symposium - PIERS*, 2017. 1, 3

[5] S. Laurens, J.P. Balayssac, J. Rhazi, G. Klysz, and G. Arliguie. Non-destructive evaluation of concrete moisture by GPR: Experimental study and direct modeling. *Materials and Structures/Materiaux et Constructions*, 38:827–832, 01 2005. 1

[6] A. Robert. Dielectric permittivity of concrete between 50 MHz and 1 GHz and GPR measurements for building materials evaluation. *Journal of Applied Geophysics*, 40:89–94, 10 1998. 1

[7] M. Schwartz, J. Garboczi, and P. Bentz. Interfacial transport in porous media : Application to dc electrical conductivity in mortars. *Journal of Applied Physics*, 78, 1995. 1

[8] A.H. Sihvola and I.V. Lindell. *Dielectric Properties of Heterogeneous Media, Chapter 3*

Polarizability modeling of heterogenous media. Elsevier, 1992. 1, 2

[9] Mohamad Achour. *Modélisation du couplage carbonatation – chlorures et étude multiéchelle de l'influence des granulats sur la diffusivité dans les bétons.* PhD thesis, Ecole Centrale Nantes, 2018. 2

[10] P. Cosenza, A. Ghorbani, C. Camerlynck, F. Rejiba, R. Guérin, and A. Tabbagh. Effective medium theories for modelling the relationships between electromagnetic properties and hydrological variable in geomaterials: A review. *Near Surface Geophysics*, 7:563–578, 10 2009. 2

[11] L.F. Chen, C.K. Ong, C.P. Neo, V.V. Varadan, and V.K. Varadan. *Microwave Electronics: Measurement and Materials Characterization.* Wiley, 2004. 3

[12] M. Stuchly and S. Stuchly. Coaxial line reflection methods for measuring dielectric properties of biological substances at radio and microwave frequencies-a review. *Instrumentation and Measurement, IEEE Transactions on*, 29:176 – 183, 10 1980. 3

[13] D. Popovic, L. McCartney, C. Beasley, M. Lazebnik, M. Okoniewski, S. C. Hagness, and J. H. Booske. Precision open-ended coaxial probes for in vivo and ex vivo dielectric spectroscopy of biological tissues at microwave frequencies. *Microwave Theory and Techniques, IEEE Transactions on*, 53:1713 – 1722, 06 2005. 3

[14] R. Zajicek, J. Vrba, and K. Novotny. Evaluation of a reflection method on an open-ended coaxial line and its use in dielectric measurements. *Acta Polytechnica*, 46(5), 2006. 3

[15] A. Boughriet, Z. Wu, H. McCann, and L. E. Davis. The measurement of dielectric properties of liquids at microwave frequencies using open-ended coaxial probes. *1st World Congress on Industrial Process Tomography, Buxton, Greater Manchester*, 1999. 3

[16] N. Wagner, T. Sokoll, and O. Schimmer. Robust low cost open-ended coaxial probe for dielectric spectroscopy in laboratory and in-situ applications. *Proceedings CMM Conference 2011*, 2011. 3

[17] N.I. Sheen and I. Woodhead. An open-ended coaxial probe for broad-band permittivity measurement of agricultural products. *Journal of Agricultural Engineering Research*, 74:193–202, 10 1999. 3

[18] K.Y. You, H. Mun, L. You, J. Salleh, and Z. Abbas. A small and slim coaxial probe for single rice grain moisture sensing. *Sensors*, 13:3652–3663, 03 2013. 3

[19] W. Skierucha and A. Wilczek. A FDR sensor for measuring complex soil dielectric permittivity in the 10-500 MHz frequency range. *Sensors*, pages 3314–3329, 01 2010. 3

[20] N. Wagner, M. Schwing, and A. Scheuermann. Numerical 3-d fem and experimental analysis of the open-ended coaxial line technique for microwave dielectric spectroscopy on soil. *IEEE Transactions on Geoscience and Remote Sensing*, 52:880 – 893, 02 2014. 3

[21] F. Demontoux, S. Razafindratsima, S. Bircher, G. Ruffie, F. Bonnaudin, F. Jonard, J.P. Wigneron, Z.M. Sbartaï, and Y. Kerr. Efficiency of end effect probes for in-situ permittivity measurements in the 0.5-6ghz frequency range and their application for organic soil horizons study. *Sensors and Actuators A: Physical*, 254:78–88, 12 2016. 3

[22] B. Filali, F. Boone, J. Rhazi, and G. Ballivy. Design and calibration of a large open-ended coaxial probe for the measurement of the dielectric properties of concrete. *Microwave Theory and Techniques, IEEE Transactions on*, 56:2322 – 2328, 11 2008. 3

[23] S. van Damme, A. Franchois, D. De Zutter, and L. Taerwe. Nondestructive determination of the steel fiber content in concrete slabs with an open-ended coaxial probe. *IEEE Transactions On Geoscience and Remote Sensing*, 42:2511–2521, 01 2009. 3

[24] D. M. Pozar. *Microwave Engineering*, volume 2. 05 2004. 3

[25] V. Guihard. *Homogénéisation de grandeurs électromagnétiques dans les milieux cimentaires pour le calcul de teneur en eau.* PhD thesis, Université Toulouse III, 2018. 3

[26] AFPC AFREM. Détermination de la masse volumique apparente et de la porosité accessible à l'eau. méthodes recommandées pour la mesure des grandeurs associées à la durabilité. *Compte-rendu des Journées Techniques, Toulouse*, 1997. 4, 5

[27] R. Snellings, A. Bazzoni, and K. Scrivener. The existence of amorphous phase in portland cements: Physical factors affecting rietveld quantitative phase analysis. *Cement and Concrete Research*, 59:139–146, 2014. 4

[28] J. Da Silva, P. Trtik, A. Diaz, M. Holler, M. Guizar-Sicairos, J. Raabe, O. Bunk, and A. Menzel. Mass density and water content of saturated never-dried calcium silicate hydrates. 31:3779, 03 2015. 4

[29] E. Gallucci, X. Zhang, and K.L. Scrivener. Effect of temperature on the microstructure of calcium silicate hydrate (C-S-H). *Cement and Concrete Research*, 48:185–195, 2013. 4

[30] P.D. Tennis and H.M. Jennings. A model for two types of calcium silicate hydrate in the microstructure of portland cement pastes. *Cement and Concrete Research*, 30(6):855–863, 2000. 4, 8

[31] I.G. Richardson. The nature of the hydration products in hardened cement pastes. *Cement and Concrete Composites*, 22(2):97–117, 2000. 4

[32] H. Jennings. Colloid model of C-S-H and implications to the problem of creep and shrinkage. *Materials and Structures*, 37:59–70, 2004. 4

[33] S.B. Jones and S.P. Friedman. Particle shape effects on the effective permittivity of anisotropic or isotropic media consisting of aligned or randomly oriented ellipsoidal particles. *Water Resources*, 36, 2000. 6

[34] J. Sanahuja, L. Dormieux, and G. Chanvillard. Modelling elasticity of a hydrating cement paste. *Cement and Concrete Research*, 37:1427–1439, 10 2007. 7, 8

[35] T. Powers. Mechanisms of shrinkage and reversible creep of hardened portland cement paste. *Proceedings of International Conference On the Structure of Concrete, Cement and Concrete*, page 319–344, 1968. 7

[36] P. Debye. Polar molecules. *The Chemical Catalog Compan*, 18, 1929. 7

[37] A. Levy, D. Andelman, and H. Orland. The dielectric constant of ionic solutions: A field-theory approach. *Physical Review Letters*, 108, 01 2012. 7